



Induced Currents in the Lining and Steel Shell of Submerged Arc Furnaces

Mads Fromreide^{1,2} · Dolores Gómez^{1,3} · Svenn Anton Halvorsen² · Pilar Salgado^{1,3}

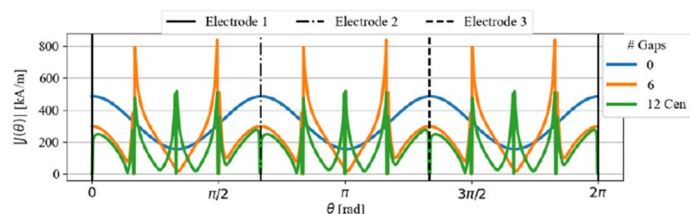
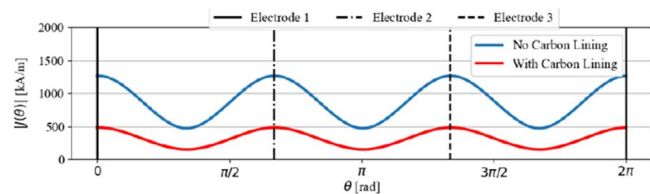
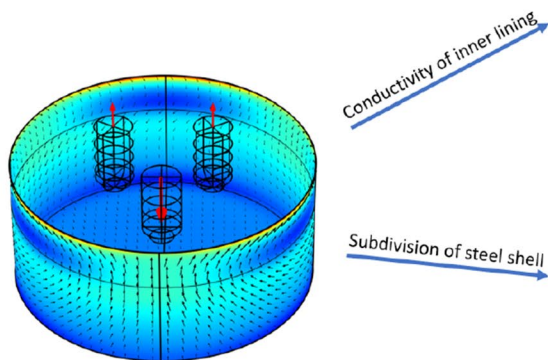
Received: 1 August 2022 / Accepted: 5 November 2022 / Published online: 17 February 2023
© The Author(s) 2023

Abstract

Numerical models in 2D and 3D are used to study induced currents in the lining and steel shell of large three-phase submerged arc furnaces. The alternating currents supplied through the electrodes cause a significant amount of induced power in the furnace lining and shell. The induced currents flow in three large loops with an accumulation of current near the top of the steel shell between the electrodes. The net result is a thermal loss with heat dissipated at the surface. Furthermore, such accumulation may cause potentially damaging hot spots in the steel. If this persists over a long time, the shell may thin and deteriorate and, in worst-case scenarios, the shell may be cracked or punctured. The influence of an electrically conducting lining and the effect of subdividing the shell in insulated sections have been studied. It is shown that an electrically conducting lining will have a significant shielding effect on the steel shell. The induced currents are considerably reduced in the steel, and “pushed into” the lining. The size of current loops in the shell can be restricted by subdividing the steel into sections with insulation between each section. Such modification is detrimental. Strong opposing currents will be formed on each side of the insulating gaps, leading to higher current concentrations and increasing the risk of hot spots on the steel shell. In addition, the heat loss due to induced currents in the steel will be enhanced.

Graphical Abstract

Induced currents create hot spots in the steel shell of three phase furnaces. The induced power depends on the material properties and the geometry of the furnace lining and shell.



The contributing editor for this article was Adam Clayton Powell.

Extended author information available on the last page of the article

Keywords Submerged arc furnaces · Electromagnetic induction · Steel shell · 2D/3D numerical simulation · Industrial electric furnace design

List of Symbols

E	Electric field	V m^{-1}
D	Electric displacement	C m^{-2}
B	Magnetic induction	T
H	Magnetic field	A m^{-1}
J	Current density	A m^{-2}
σ	Electric conductivity	S m^{-1}
ϵ	Electric permittivity	F m^{-1}
μ_0	Magnetic permeability of vacuum	H m^{-1}
μ_r	Relative permeability	-
μ	Material permeability, $\mu = \mu_r \mu_0$	H m^{-1}
f	AC frequency	Hz
δ	Skin depth, $\delta = 1/\sqrt{\pi f \mu_r \mu_0 \sigma}$	m
ω	Angular frequency, $\omega = 2\pi f$	s^{-1}

Introduction

The current patterns within large, three-phase submerged arc furnaces (SAFs) are to a large degree influenced by electromagnetic induction. In this work, we will focus on the conditions in the periphery. Here, large current loops are induced in a conductive (carbon) lining and in the surrounding steel shell. Such currents generate heat where cooling is needed and potentially damaging hot spots can be found where the currents concentrate on the steel shell. Among others, we will investigate a question raised in discussions with the industry: Will the conditions improve if smaller current loops are enforced by subdividing the steel shell into sections?

In a typical (cylindrical) SAF, three electrodes are arranged in an equilateral triangle, each carrying alternating current (AC) in a three-phase set-up. SAFs are used in the production of most ferro-alloys. The energy required for the process is supplied through the electrodes, carrying high-intensity AC at the grid frequency (typically 50 or 60 Hz). The models presented in this work are based on cylindrical three-phase furnaces for ferromanganese (FeMn) production. The general results will, however, be applicable to other processes. The FeMn production process is characterized by having coke-enriched regions, known as coke beds, surrounding the tip of the electrodes. The coke particles within the coke bed act as both electric resistors and as a reduction agent for the final reduction step [1]. The required energy for the process is generated by ohmic heating in the furnace hearth. In other processes, for instance (ferro)silicon production, the energy is mainly generated by electric arcs below

the electrode tips [2]. The production process is complex and involves various materials (solids, liquids, gases). The distribution of electric current and power has a large influence on the furnace conditions. Thus, a proper understanding is vital for design, operation, and control of the production process. Improved electrical conditions will directly lead to a more stable process with better efficiency and help ensure an economically and environmentally sustainable primary metal production.

For a given frequency, the distribution of alternating current in a conductor depends on the geometry and the material properties. The distribution will, in general, be governed by the ratio $(L/\delta)^2$ [3], where L is a characteristic dimension and δ is the material skin depth. The skin depth is defined as $\delta = 1/\sqrt{\pi f \mu \sigma}$, where f is the AC frequency, μ the magnetic permeability, and σ the electric conductivity [4]. In good conductors, the current concentrates near the surface in a layer of thickness δ ; this effect is known as the *skin effect*. The skin effect is caused by internal induction. The effect is equivalent to a reduction of the cross-sectional area and, therefore, the effective resistance is increased. The current distribution will also be affected by the mutual inductance with currents in nearby conductors (proximity effect).

The skin and proximity effects in electrodes of three-phase SAFs have been extensively studied with both 2D models [5–10] and 3D models [5, 11–17]. In most works, the steel shell that surrounds the furnace is not included in the computational domain. Since the steel shell is comparatively thin with a large surface area, it will considerably increase the computational cost to fully resolve it. The main task of the steel shell is structural, i.e., to provide a suitable casing for the furnace. However, the structural steel is both highly conductive and (usually) ferromagnetic. Thus, large eddy currents will be induced [1, 5, 11].

The shell currents are mainly due to induction from the high-intensity currents of the electrodes. This will in turn cause a proximity effect between the electrode currents and the shell currents competing with the electrode–electrode proximity effect [5, 11], and thus make an impact on the inner conditions. Between the steel shell and the inner part of the furnace, there is a lining, typically consisting of both conductive (carbon) and non-conductive layers (ceramics). There will be interactions between induced currents in the steel and currents in the conductive layers, depending on their material properties and geometry [3, 18].

The induced currents on the inside of the steel shell, flow in three large loops, vertically behind each electrode and

closing horizontally between the electrodes. At the bottom, the current loops are wide, while they concentrate near the inner top of the steel shell [5]. This leads to significant heat dissipation at the shell (loss of power) and the subsequent need for active water cooling. If this situation persists over a longer time period, the steel may thin and deteriorate due to oxidative damage. In worst-case scenarios, the steel may be cracked or punctured resulting in the risk of uncontrolled gas leakage, reduced process efficiency, unwanted production stops for repairs, and potentially a shorter lifetime for the furnace.

To improve the conditions, it was assumed that smaller current loops might reduce the induced currents and the accompanying heat generation.

Since the currents in the steel shell are mainly caused by the vertical electrode currents, 2D models with out-of-plane currents can quantitatively describe the mechanisms, especially in the upper part. But the 2D models will overestimate the intensity of the shell currents and 3D models are required for accurate solutions [5]. In this work, we apply both 2D models with out-of-plane currents as well as full 3D models. 2D models are much less computationally costly than 3D models and are very useful to acquire qualitative insight. In many cases, simple 2D models can contribute to a better understanding of the governing mechanisms, compared to more complex 3D models. In particular, the mutual inductance (proximity effect) between the shell currents and electrode currents can effectively be studied by 2D models.

This work focuses on the induced currents and power in the conductive linings and steel shell of SAFs. We have investigated the effect of modifying the lining and the impact of subdividing the steel shell. The main objective is to analyze if such structural changes would lead to energy savings and less wear of materials, and therefore, to a more sustainable production. The models are based on realistic dimensions for industrial FeMn furnaces found in the literature [11].

In Sect. “Furnace Model,” the geometry of the furnace is described. In Sect. “Mathematical Model,” the basics of the modeling are summarized. Section “Numerical Simulations” presents the numerical results. A short discussion is given in Sect. “Discussion” while the conclusions are given in Sect. “Conclusions.”

Furnace Model

Three-phase AC furnaces are used in the production of different ferro-alloys such as ferromanganese and ferrosilicon. Figure 1 shows a 3D sketch of the geometry. Briefly, it consists of a cylindrical shell with three cylinder-shaped electrodes submerged in the charge material. An alternating current is applied through the top of the three electrodes with

120° electrical phase shift between them. The electrodes, consisting of good conductors, carry the electric currents to the center of the furnace where the main chemical reactions take place. Indeed, the energy developed in the furnace is used to melt and reduce oxides to metal.

The interior of the furnace can be divided into different regions, mainly the inner layers, coke beds, linings, and surrounding steel shell that can be also appreciated in Fig. 1. These regions are described in detail in Fig. 2. In particular, we can distinguish a first part with charge components (mixture) at different temperatures (zones 3, 4, and 5), where electrodes (zone 2) are buried, the coke bed (zone 6) and at its bottom, a layer with the resulting alloy. The term coke bed denotes the enriched area between the electrode tip and the metal bath (zone 7), where the oxides are liquid. The coke beds are modeled as half-ellipsoids which are connected/overlapping at the furnace center. Most industrial furnaces have a furnace shell. Its function is to carry the weight of the furnace, and it is typically made of structural steel. In the 3D computational domain, the geometry of the steel shell, which is usually very thin, has been simplified to a straight cylindrical shell in order to avoid its extremely fine discretization as it was done in [11].

The model neglects the steel lid/roof of the furnace which has no importance in the study we intend to perform (for details on induced currents in the steel roof, we refer the reader to [11]). For the same reason, the baking zone, electrode clamps, electrode casing, busbars, and flexibles are not considered. The model also assumes that the regions of interest, namely, the steel shell and carbon linings of the furnace, are continuous and isotropic, and any transition zones such as welded joints in the steel shell and cracks in the linings have not been accounted for. The raw materials in the interior are in general granular. However, for simplicity, they are treated as uniform using reasonable average bulk properties. This is a common approach for large-scale furnace models. Some work has been done to determine the electrical and thermal conductivity through granular materials and used homogenized models in a metallurgical context [19, 20].

The dimensions of the furnace model are based on the description of industrial FeMn furnaces given in [11, 21]. The full furnace diameter is set to 14 m, the electrode diameter is set to 1.9 m and the electrode distance (center-center) is set to 4.9 m. The steel shell thickness is fixed to 2.5 cm, while the thickness of the carbon lining is 65 cm. The electrode tip position is set to 1.815 m (above the alloy), which results in reasonable values for power and resistance in industrial furnaces [11]. A complete description of the geometric parameters are given in Table S1 in the electronic supplementary material.

Table 1 lists the main material properties of the different parts, which are based on values given by [11, 21, 22]. To

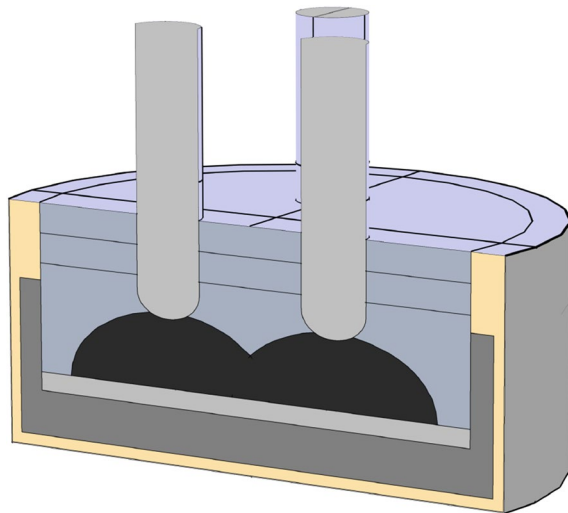


Fig. 1 Geometry of the 3D model of a three-phase furnace (the surrounding air is neglected)

avoid the coupling with a thermal model, which is not the goal of this work, all the material properties are assumed to be constant. Nevertheless, to account for the different temperature zones inside the furnace, the charge is divided into three layers of increasing conductivity related to the increased temperature [11, 21]. On the other hand, the steel shell, which is usually a ferromagnetic material, has been simplified to a linear magnetic material with constant magnetic permeability.

As mentioned in the introduction, 2D numerical simulations will also be performed. The geometry of the 2D model is shown in Fig. 3, where the numbering of the different material regions follows Table 1. Notice that this 2D geometry refers only to the upper part of the furnace where the current can be assumed to be vertical.

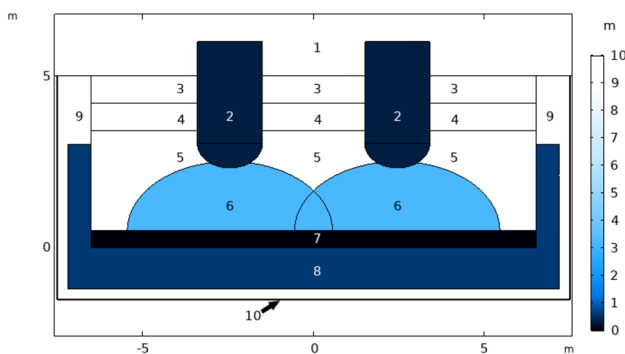


Fig. 2 2D cut plane of the 3D furnace model, showing the different material regions: 1. air, 2. electrodes, 3. charge mix 400 °C, 4. charge mix 800 °C, 5. charge mix 1200 °C, 6. coke beds, 7. alloy, 8. carbon lining, 9. oxide lining, 10. steel shell. The colors indicate the skin depth in conducting materials ($\delta = 1/\sqrt{\pi f \mu \sigma}$) at 50 Hz, with the scale restricted to 10 m (Color figure online)

Mathematical Model

Electromagnetic fields are governed by Maxwell’s equations. Since the current supplied to the electrodes is alternating, it varies sinusoidally in time and we can use a time-harmonic approach if, as is the case, the materials composing the furnace are assumed to be magnetically linear. Namely, we can consider that all electromagnetic fields vary harmonically with time in the form:

$$F(x, t) = \text{Re}(e^{i\omega t} F(x)),$$

where Re denotes the real part of its argument, i is the imaginary unit, $\omega = 2\pi f$ is the angular frequency, and $F(x)$ is the time-independent complex amplitude of the field. Thus, the electromagnetic fields inside the furnace are accurately described by the time-harmonic Maxwell’s equations:

$$i\omega B + \text{curl}E = 0, \tag{1}$$

$$i\omega D - \text{curl}H = -J, \tag{2}$$

$$\text{div} B = 0, \tag{3}$$

$$\text{div} D = \rho_V, \tag{4}$$

$$B = \mu H, \tag{5}$$

$$D = \epsilon E. \tag{6}$$

In the equations above, all fields are written in terms of its complex amplitude and the usual notation has been adopted: B is the magnetic induction, H the magnetic field, E the electric field, D the electric displacement, J the current density, ϵ the electric permittivity, μ the magnetic permeability, and ρ_V the free charge density. In these furnaces, there is no accumulation of charge, so we can assume $\rho_V = 0$.

Table 1 Material properties (from [11]): electric conductivity σ , relative magnetic permeability μ_r , and skin depth δ (at $f = 50$ Hz)

Material	σ [S/m]	μ_r [1]	δ [m]
Electrodes (2)	5×10^4	1	0.32
Charge mix 400 °C (3)	0.075	1	260
Charge mix 800 °C (4)	0.15	1	180
Charge mix 1200 °C (5)	15	1	18
Coke beds (6)	500	1	3.2
Alloy (7)	1.5×10^5	1	0.18
Carbon lining (8)	1.4×10^4	1	0.60
Oxide lining (9)	1×10^{-6}	1	7.1×10^4
Steel shell (10)	3×10^6	100	0.0041

The numbers in parenthesis refer to definitions in Fig. 2

Moreover, in conductors, \mathbf{J} is related to \mathbf{E} through Ohm’s law:

$$\mathbf{J} = \sigma \mathbf{E}, \tag{7}$$

where σ is the electrical conductivity.

As the operating frequency is low, typically 50 or 60 Hz, the term involving the electric displacement could be neglected in the Maxwell–Ampère law, which is a solution frequently used in the literature (see [7–9] for instance). However, we are going to use COMSOL Multiphysics software package to approximate the fields, and in particular, the so-called *Magnetic and Electric Field* module [23] which actually solves the full Maxwell system described above. Namely, this interface formulates the problem in terms of an electric scalar potential V and a magnetic vector potential \mathbf{A} defined by $\mathbf{B} = \text{curl } \mathbf{A}$ and $\text{grad } V = -\mathbf{E} - i\omega \mathbf{A}$ (the so-called A-V formulation). In this context, the computational effort in the frequency domain for solving the full Maxwell system is equivalent to that required for solving the eddy current model.

The equations above are numerically solved by using a finite element method. Hence, we restrict them to a bounded domain and to impose proper boundary conditions on the magnetic field, a large volume of air is considered around the furnace. Thus, the computational domain consists of two parts: one occupied by conductors (the electrodes and the materials inside the furnace) and other occupied by the dielectric (the air around the conductors).

In the 3D geometry, the outer boundary of the conducting domain has three components corresponding to the top of the electrodes where the current will be prescribed. For two of the electrodes the total current with a phase shift of

120° is fixed, and for the third one, the current is automatically computed by current conservation. Moreover, in the numerical simulations, the boundary conditions are fixed by a given amplitude I_a of the AC. In general, the exact value of I_a will scale the resulting field distributions, but not change their qualitative behavior. The value of I_a is fixed to 190 kA based on the value used in [11], which is considered to be reasonable for the given furnace size. In the rest of the outer boundary, the magnetic insulation boundary condition was used.

On the other hand, as it was advanced in the previous section, in the 3D model, the geometry of the steel shell was simplified to a straight cylindrical shell. Given that the steel shell is very thin, it is computationally costly to consider a suitable discretization in 3D. Therefore, we have applied an impedance-type boundary condition [23, 24]. That is, the condition

$$\mathbf{n} \times \mathbf{E} = Z_\omega \mathbf{n} \times (\mathbf{n} \times \mathbf{H}) \tag{8}$$

is added to the 3D model, and applied to the surface of the steel shell. The surface impedance Z_ω is defined as $Z_\omega = \sqrt{\mu/(\epsilon - i\sigma/\omega)}$ [24]. This methodology that has previously been validated for the steel shell of SAFs [11], allows for the steel shell to be treated as a surface, thus, reducing the high computational cost of fully resolving its thin volume. Hence, the induced currents in the steel shell have been modeled as surface currents.

Concerning the 2D model, the main assumption is that the current density only has non-null component in the z-direction, that is, it has the form: $\mathbf{J} = J_z(x, y)\mathbf{e}_z$, which is suitable in the upper part of the furnace. This assumption is the one considered in the so-called “out of plane model” in COMSOL. In this case, the boundary condition on the whole boundary of the computational domain is a magnetic insulation condition. Additionally, the electrical source must be imposed with some constraints; namely, the total current through each electrode will be given. On the other hand, in the conducting sections of the steel, it is also needed to provide the current or the voltage; we will consider that the total current through the steel shell is null, due to the fact that the shell is modeled as an infinite conductor which does not close a circuit [25]. For the cases where the steel shell is divided in insulated sections (see Fig. 4), the total current in each section is also null.

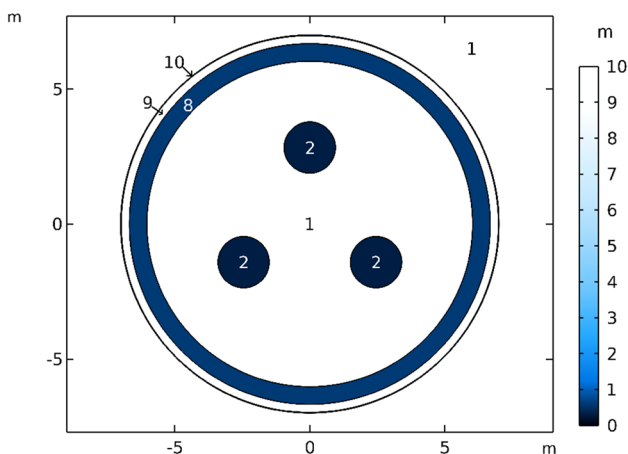


Fig. 3 Geometry of the 2D model. The different materials are denoted with the same numbers as in Fig. 2. The colors indicate the skin depth in conducting materials at 50 Hz, with the scale restricted to 10 m (Color figure online)

Numerical Simulations

As mentioned in the introduction, the material composing the steel shell is highly conductive, and strong eddy currents are induced in it which may also modify the currents of the electrodes. We are interested in analyzing the effect of

some structural modifications of the furnace on the current distribution and power dissipation in the steel shell and carbon lining. To attain this goal, we have performed different simulations where either the steel shell or the carbon lining or both of them have been modified in some sense. More precisely, the simulations comprise five 2D simulation cases and six 3D simulation cases which have been summarized in Table 2. In 2D, we have considered two cases with solid steel shell with or without the conductive carbon lining present. Further, we have considered one case with six gaps in the steel shell and two cases with twelve gaps in the shell. The two cases with twelve gaps differ by the gap position which is either placed symmetrically about or centered behind the electrodes. In the six-gap case, the insulating gaps are placed symmetric about the electrodes. The positions of the insulated gaps relative to the electrodes are shown in Fig. 4.

In 3D, we have considered a reference case (Case 6) based on the geometry in [11]. Further, we have considered three cases where the carbon lining is extended vertically, so that it has the same height as the steel shell. In these three cases, the thickness of the full side wall of the carbon lining is varied. In the last two cases, we have considered subdividing the steel shell by including six vertical insulating gaps and two horizontal gaps spanning the whole periphery of the steel shell. The vertical gaps are placed centered or symmetric about the electrodes. In both cases, the horizontal insulating gaps are kept fixed, so that the upper is placed slightly above the electrode tip, while the other is placed underneath the tip. This means that the upper section will experience most induction from the electrode current, the middle will experience some induction from the electrodes, while the bottom section will not be subject to significant induction from the electrode currents.

In addition, we have considered the effect of the size of the insulating gaps by analyzing 2D simulations with varying gap sizes. The gap size has been varied between 0.1° and 1.5° , corresponding to about 1 cm and 15 cm, for

Table 2 Cases considered in the 2D (from 1 to 5) and 3D (from 6 to 11) simulations

Case	No. shell divisions (vert.)	C-lining	C-lining thickness (m)	Gap positions
1	0	Not included	0.65	–
2	0	Included	0.65	–
3	6	Included	0.65	Symmetric
4	12	Included	0.65	Symmetric
5	12	Included	0.65	Centered
6	0	Included	0.65	–
7	0	Extended	0.65	–
8	0	Extended	0.30	–
9	0	Extended	0.10	–
10	6	Included	0.65	Symmetric
11	6	Included	0.65	Centered

Reference case for the 3D simulations is number 6

a 2D model with twelve gaps in the steel shell. The gaps are placed symmetric around the electrodes (Case 4) and both with and without carbon lining has been considered. We have observed that the effect of the size of the insulating gaps is small. The change in dissipated power has been observed to be very small for different gap sizes (within the given range). Moreover, the change is localized in the steel shell (see Table S2 of the electronic supplementary material). That is why in the present work we only consider a gap size of 1° which corresponds to about 10 cm for the given furnace diameter. The horizontal gaps of the 3D model have also been fixed to 10 cm.

2D Simulation Results

In Fig. 5, the norm of the magnetic induction $|\mathbf{B}|$ is shown for the 2D model with and without the conducting carbon lining (cases 1 and 2, respectively). While the distributions

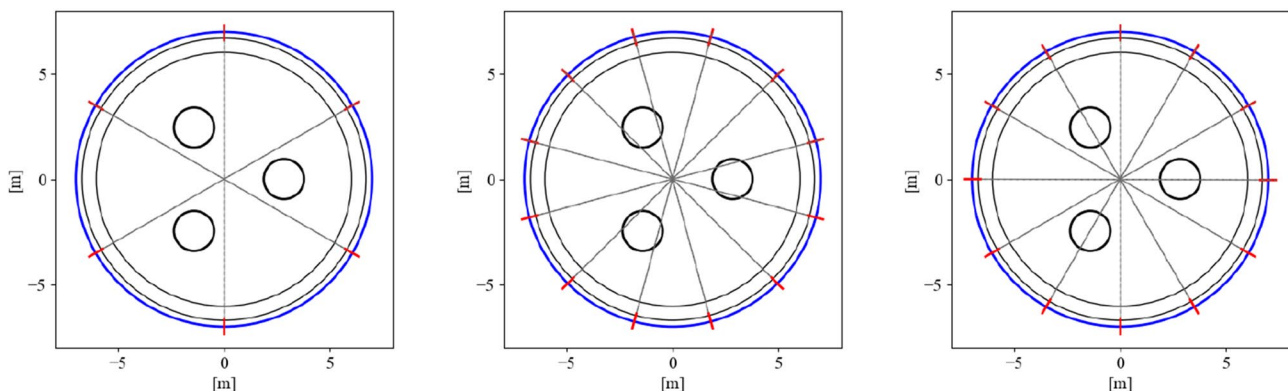


Fig. 4 Positions of insulated gaps (in red) in the steel shell (in blue) for the 2D model. Left: 6 gaps symmetric, middle: 12 gaps symmetric, right: 12 gaps centered (Color figure online)

are similar in the center, we observe clear differences in the outer region. For the case with no carbon lining (Case 1), the field strength at the outer steel shell is stronger than in the case with carbon lining (Case 2). However, the introduction of the conducting lining increases the field strength considerably near its inner boundary, thus, increasing the concentration towards the center. The effect on the induced steel shell currents is visualized by considering the induced currents on the *inside* of the steel shell. Figure 6 shows the norm of the current density on the inner circumference of the steel shell for cases 1 and 2. The curves show how the induced shell currents are damped by the carbon lining.

Figure 7 shows the current density norm on the *inside* of the steel shell when the shell is subdivided into insulated sections (cases 3, 4, and 5 in Table 2). Both plots include the curve for a solid steel shell (same as in Fig. 6) with the carbon lining included (Case 2). The top plot corresponds to the twelve-gap case with the gaps symmetric around the electrodes (Case 4), and the bottom plot to the twelve-gap case with the gaps centered on the electrodes (Case 5). The positions of the gaps in the six-gap case (Case 6) are the same in both plots. The figure shows how the insulated gaps create local spikes in the current norm on both sides of the insulating material.

3D Simulation Results

Figure 8 shows the induced current on the *inside* of the steel shell in the full 3D model (cases 6 and 7). The color indicates the norm of the current, while the black arrows

indicate the current direction. The red arrows in each electrode illustrate the direction of the total current in each electrode. The length of the red arrows reflects the intensity in the electrodes. However, the red and black arrows are scaled individually. For each of the plots, the time instant for the arrows is chosen so that there is maximum current in the front electrode which distributes equally to the other two electrodes. The plot in the top shows the (reference) Case 6, that is, neither shell divisions nor extended carbon lining is considered. The bottom plot shows the case where the carbon lining is vertically extended to the top of the steel shell (Case 7). For the reference case, we observe how vertical currents are induced behind each electrode, in the opposite direction relative to the nearest electrode. The currents close in loops and move horizontally, at the top and bottom, between the electrodes. There are significant current accumulation in the top of the shell, between the electrodes with a risk of creating hot spots. This distribution agrees well with the results found by Herland, Sparta, and Halvorsen in [11]. For the case considering the extended carbon lining, the intensity of the current is reduced significantly, and the accumulation in the top is less visible. The direction of the current distribution is similar in both cases.

The current distribution on the *inside* of the steel shell is plotted in Fig. 9 for the two cases with subdivided steel shell (cases 10 and 11). As in Fig. 8, the color range has been restricted to 10 kA/m for both cases. The 3D simulations show similar behavior to the 2D case, with a large local increase in the current density norm near the insulated

Fig. 5 Magnetic induction norm: left, when the carbon lining is neglected (case 1); right when the carbon lining is included (case 2). The color range is limited to 15 mT to resolve the outer parts (Color figure online)

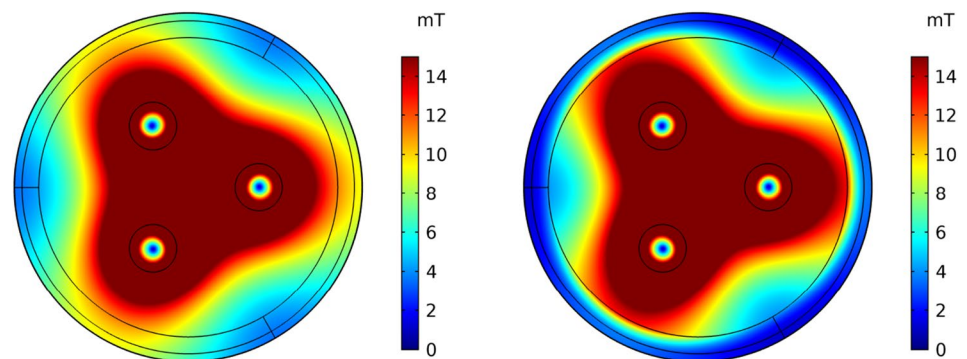


Fig. 6 Current density norm on the inner circumference of the steel shell with and without carbon lining present (cases 2 and 1, respectively). The vertical lines indicate the position of each electrode

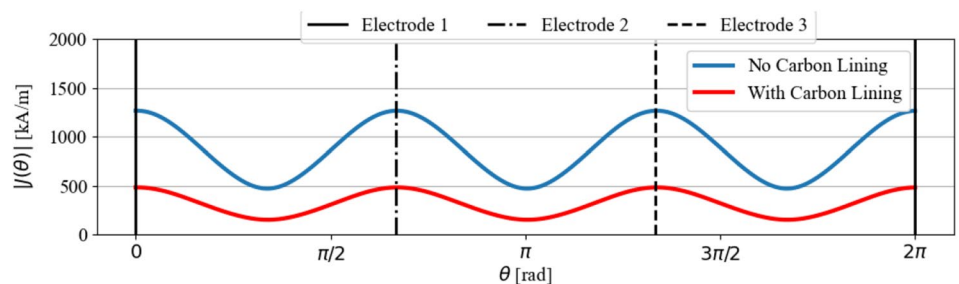
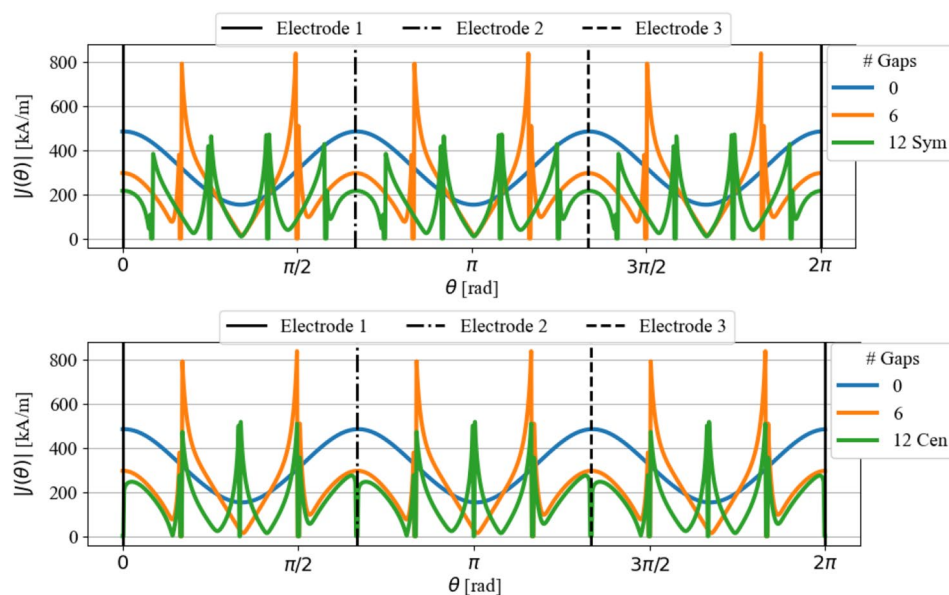


Fig. 7 Current density norm on the *inside* of the steel shell with 0, 6, and 12 insulated sections. Case 2 and 3 are included in both plots; Case 4 (12 gaps symmetric) in the top and Case 5 (12 gaps centered) in the bottom



gaps. The hot spots are created both along the vertical and horizontal gaps.

The different positioning of the insulating gaps gives rise to some changes in the current distributions. Compared with the reference case with solid steel shell (Fig. 8), the sub-sectioning cases give a significant increase in the total induced current.

As a measure of the impact of the different models on the steel shell and linings, we have calculated the total electric power in the various parts of the furnace and the total for each 3D case. Thus, we have considered the power dissipated in the steel shell (P_s), carbon lining (P_c), electrodes (P_e), remaining interior (P_{interior}), and total power (P_{total}). For the steel shell, the value is given by the surface loss density on the steel shell surface, associated with the calculated surface currents. For remaining parts, the electric power is calculated as the usual volumetric power, $P = |\mathbf{J}|^2 / (2\sigma)$. The results are summarized in Table 3. From these results, we see that the total power is comparable for all cases, with an increase of about 1.6% from the reference case (Case 6) to the highest cases (cases 10 and 11). This increase comes mainly from the induced power in the carbon lining. Further, we deduce that the extended carbon lining (in height) reduces the induced power in the steel shell; this is true even when the thickness (of the full sidewall) is reduced to 0.10 m. Simultaneously, we see that there are more power induced in the carbon lining. For the two cases where the steel shell is subdivided (Case 10 and 11), we see an increase in the total power induced in the steel shell. However, the impact on the carbon lining is much more prominent, as the total induced power is more than doubled. There is also a small increase in the electrodes and interior for these cases.

Discussion

Electromagnetic induction follows the general principle that nature resists changes, in this case: a change in the magnetic field in a conductor will induce a voltage (an E-field) to create a current that will counteract the change in the magnetic field.

For good conductors, the magnetic field is largely reduced in the interior and the current is concentrated on the boundaries. Generally, parallel currents in the same direction “are pushed away” from each other [4]. By Ampere’s law, the alternating magnetic fields far away from the conductors are given by the total current. The cyclic changes in the magnetic field are best reduced by moving the currents away from each other.

Parallel currents in opposite directions “are moved towards” each other [4]. The magnetic fields from opposing currents will counteract each other, and the cyclic changes in the magnetic field are reduced when the opposing currents are close.

It might be thought that reducing the size of the current loops would reduce the concentration of induced currents. The simulations show, however, strong, opposing current loops with enhanced current concentrations (Figure S3). Hence, in three-phase electric furnaces, insulating gaps would imply higher risk for hot spots and increased heat loss due to the associated electric power from the eddy currents on the steel shell.

The effect of the gap size between the sections was investigated by some 2D simulations. The general trend is more concentrated currents on each side of the gap when the gap is reduced. The power generated in the steel shell will increase correspondingly. Other effects are minor. Based on

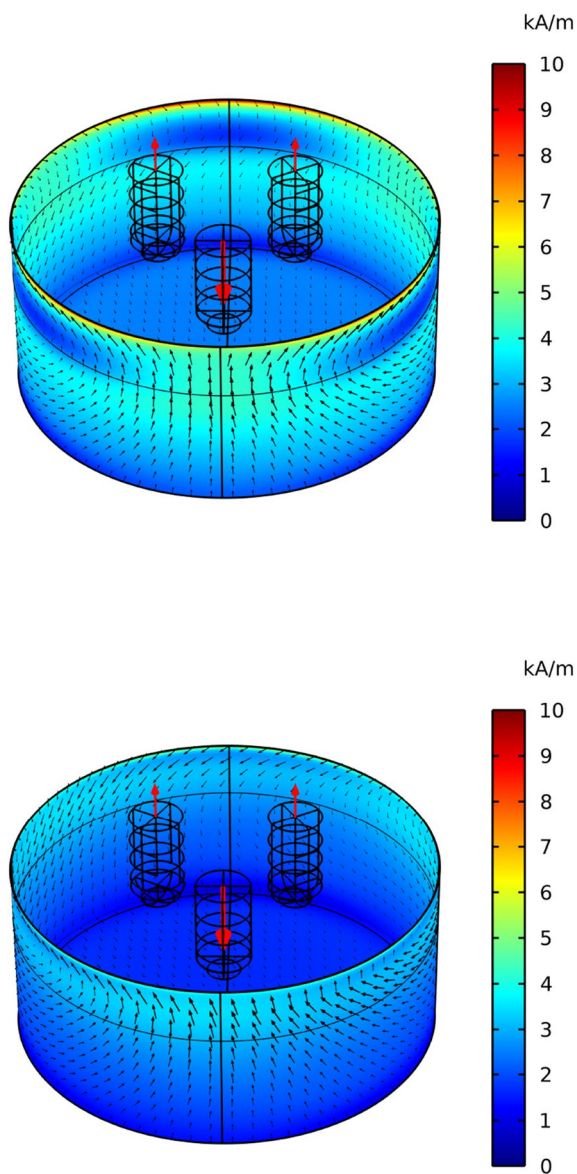


Fig. 8 Current on the *inside* of the steel shell for the 3D reference case (Case 6) (top), extended height of carbon lining (Case 7) (bottom). The color range is restricted to 0–10 kA/m and shows the surface current density norm. The black arrows indicate the pattern of the shell current at a time instant. The red arrows indicate the direction of the electrode currents (Color figure online)

this result, it was decided that variation of the gap size was not required for the remaining cases. A comparatively large gap size of $1^\circ/10$ cm was chosen. Then very small elements are not required in the gaps, which would have implied more computational time.

The simulations show that the carbon lining has a shielding effect. Induced currents in the lining imply far less induction in the steel shell. There is a strong proximity effect between parallel currents in adjacent conductors. The electric current is generally “pushed away” from the good

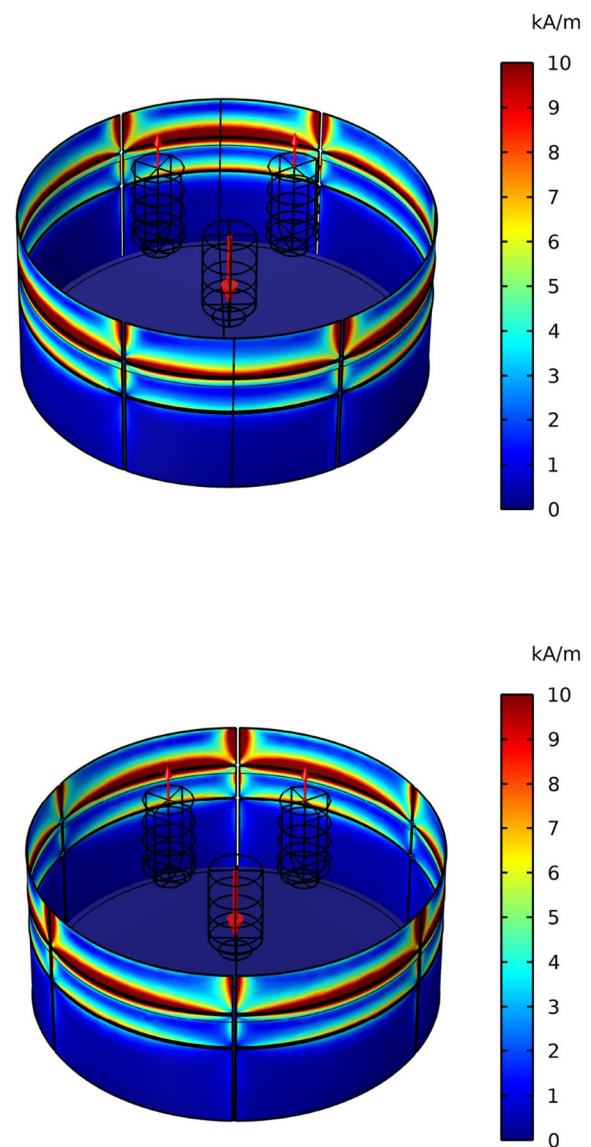


Fig. 9 Current on the *inside* of the steel shell when both vertical and horizontal insulation gaps are included. The vertical insulation gaps are placed symmetric (Case 10) about the electrodes (top) and centered (Case 11) behind the electrodes (bottom). The color range is restricted to 0–10 kA/m and shows the surface current density norm. The red arrows indicate the direction of the electrode currents (Color figure online)

conductor (here: steel) into less conductive material (here: carbon) [3]. In our simulations, we have assumed proper electrical contact within the lining and between the lining and the steel shell. If not, the paths of the induced currents will be restricted with potentially unfavorable effects.

The simulations demonstrate a general learning that simple models (here: 2D models) are very valuable to study the basic effects. The 2D models demonstrate clearly that there will be induced currents (in the lining and steel shell) behind each electrode, where the induced currents will be opposite

Table 3 Total heat loss density (in MW) in steel shell (surface), carbon lining, electrodes, and interior for the 3D simulations

Case	P_s	P_c	P_{s+c}	P_e	P_{interior}	P_{total}
6	0.29	0.33	0.62	2.63	36.59	39.84
7	0.10	0.53	0.63	2.61	36.55	39.79
8	0.15	0.53	0.68	2.62	36.59	39.89
9	0.22	0.39	0.61	2.63	36.63	39.87
10	0.32	0.69	1.01	2.74	36.75	40.50
11	0.31	0.69	1.00	2.74	36.75	40.49

to the respective electrode currents. Further, the shielding effect of a carbon lining, the unfavorable effect of sectioning the steel shell, and the influence of the gap size are clearly seen. But some effects cannot be studied with the assumptions of the 2D model (strictly, vertical current). 3D models are for instance required to compute how the current loops closes, and to include both vertical and horizontal insulating gaps. Also, full 3D models are required to get results that can be applied to study details of the furnace design, e.g., thickness and height of a carbon lining.

The steel shell has been treated as a linear magnetic material with constant magnetic permeability. Some simple test calculations have shown that constant magnetic permeability works well and produces the same general results as a (more expensive) non-linear model that includes magnetic saturation. The results for a linear model can be improved by adapting the relative magnetic permeability to the actual size of the magnetic fields. This will require a separate study which is not the goal of this work.

The induction in the steel shell and a conductive lining cannot be avoided. But it can be controlled in the sense that modifications are possible by proper design. We recommend that electrical simulations are performed for actual furnace designs. In such computations, all relevant details need to be included. There will, for instance, be induced currents in a steel roof. Here, effects of opposing currents can be seen, due to the insulating “gap” between the lid and the furnace casing, see for instance Herland, Sparta, and Halvorsen [11].

The insulating gaps could also be considered as parts of the shell where the steel has been degraded. The results show how this leads to vicious loop, where degraded steel gives raise to hot spots which will further degrade this part, making the problem worse.

Conclusions

Electromagnetic simulations have successfully been applied to study induced currents in the lining and steel shell of three-phase submerged arc furnaces. Strong vertical currents are induced behind each electrode. The induced currents form three large loops, with horizontal currents between the electrodes at the top of the steel shell and below the

electrode tips. At the top, there are strong current concentrations with corresponding risk of (damaging) hot spots.

Restricting the size of the current loops has a detrimental effect. If the steel shell is sectioned with (electrically) insulating gaps, strong opposing currents will be formed on each side of the gaps, implying more heat loss and higher risk of damaging hot spots.

The induced currents in the steel shell will be modified by an electrically conductive lining. Such lining has a shielding effect, reducing the currents in the steel shell.

We recommend electromagnetic simulations as part of furnace design studies, for instance to study the effect of the height and width of an electrically conductive lining. This may contribute to furnace designs with less undesired power dissipation due to induction, heat losses, and need for water cooling. Furthermore, the operation lifetime and the uptime may be extended if advanced electromagnetic analysis is taken into consideration in early stages of the design. All these improve the economical and environmental sustainability of the furnace processes.

Supplementary Information The online version contains supplementary material available at <https://doi.org/10.1007/s40831-022-00625-6>.

Acknowledgements This paper is published as part of the project Electrical Conditions and their Process Interactions in High-Temperature Metallurgical Reactors (EIMet) with financial support from The Research Council of Norway (Pr. No. 247791) and the companies Elkem and Eramet Norway. The work has also been supported by the project “Electrical Conditions in Submerged Arc Furnaces - Identification and Improvement” (SAFECI), with financial support from The Research Council of Norway (Pr. No. 326802) and the companies Elkem, Eramet Norway, Finnjord, and Wacker Chemicals Norway. The authors affiliated to CITMaga have also received funding from Xunta de Galicia (Pr. No. GI-1563 ED431C 2021/5) and FEDER, Ministerio de Ciencia e Innovación-AEI research project PID2021-122625OB-I00.

Funding Open Access funding provided thanks to the CRUE-CSIC agreement with Springer Nature.

Declarations

Conflict of interest On behalf of all authors, the corresponding author states that there is no conflict of interest.

Open Access This article is licensed under a Creative Commons Attribution 4.0 International License, which permits use, sharing, adaptation, distribution and reproduction in any medium or format, as long


as you give appropriate credit to the original author(s) and the source, provide a link to the Creative Commons licence, and indicate if changes were made. The images or other third party material in this article are included in the article's Creative Commons licence, unless indicated otherwise in a credit line to the material. If material is not included in the article's Creative Commons licence and your intended use is not permitted by statutory regulation or exceeds the permitted use, you will need to obtain permission directly from the copyright holder. To view a copy of this licence, visit <http://creativecommons.org/licenses/by/4.0/>.

References

- Olsen S, Tangstad M, Lindstad T (2007) Production of manganese ferroalloys. Tapir Academic Press, Trondheim
- Gasik M (2013) Handbook of ferroalloys: theory and technology. Elsevier, Amsterdam
- Fromreide M, Gómez D, Halvorsen SA, Herland EV, Salgado P (2021) Reduced 2D/1D mathematical models for analyzing inductive effects in submerged arc furnaces. *Appl Math Model* 98:59–70
- Lupi S (2017) Fundamentals of electroheat. Springer, Cham
- Herland E, Sparta M, Halvorsen S (2019) Skin and proximity effects in electrodes and furnace shells. *Metall Mater Trans B* 50:2884–2897
- Innvær FK, R. and T. Sira (1985) Three-dimensional calculations on smelting electrodes. In: Proceedings from the 43rd electric furnace conference, Atlanta, GA, 10–13 December, pp. 265–272
- Bullón J, Lage M, Bermúdez A, Pena F (1998) The new compound electrode: current situation and thermoelectric studies. In: Proceedings of INFACON VIII, vol 8
- Bermúdez A, Muñiz MC, Pena F, Bullón J (1999) Numerical computation of the electromagnetic field in the electrodes of a three-phase arc furnace. *Int J Numer Methods Eng* 46(5):649–658
- Palsson H, Jonsson M Finite element analysis of proximity effects in Sderberg electrodes. <https://www.hi.is/magnusj/ritverk/proxi/mit.pdf>. Accessed 10 May 2022
- Larsen H (2007) Current distribution in the electrodes of industrial three-phase electric smelting furnaces. In: Proceedings of the 2006 Nordic COMSOL conference, Copenhagen, Denmark
- Herland E, Sparta M, Halvorsen S (2018) 3D models of proximity effects in large FeSi and FeMn furnaces. *J South Afr Inst Min Metall* 118(6):606–618
- Mc Dougall I (2007) Finite element modelling of electric currents in AC submerged arc furnaces. In: Infacon XI: International Ferro-Alloys Congress, New Delhi, India
- Tesfahunegn YA, Magnusson T, Tangstad M, Saevarsdottir G (2019). Dynamic current and power distributions in a submerged arc furnace. In: Lambotte G, Lee J, Allanore A, Wagstaff S (eds) *Materials processing fundamentals* 2019. Springer, Cham, pp 3–14. https://doi.org/10.1007/978-3-030-05728-2_1
- Tesfahunegn YA, Magnusson T, Tangstad M, Saevarsdottir G (2020). The effect of side arcs on current distributions in a submerged arc furnace for silicon production. In: Lee J, Wagstaff S, Lambotte G, Allanore A, Tesfaye F (eds) *Materials processing fundamentals* 2020. Springer, Cham, pp 177–188. https://doi.org/10.1007/978-3-030-36556-1_16
- Tesfahunegn Y, Magnusson T, Tangstad M, Saevarsdottir G (2020) Comparative study of AC and DC solvers based on current and power distributions in a submerged arc furnace. *Metall Mater Trans B* 51(2):510–518
- Innvær FKR, Sira T (1987) 3-Dimensional calculations on smelting electrodes. *MIC* 8(2):103–115
- Yu Y, Li B, Yun C, Qi F, Liu Z (2021) Modeling on reduction reaction of metal oxides for submerged arc furnace in ferrochrome pellets smelting process. *Metall Mater Trans B* 52(6):3907–3919
- Fromreide M, Halvorsen SA, Sparta M, Risinggård VK, Salgado P, Gómez D, Herland EV (2021) Effects of alternating currents in the hearth of submerged arc furnaces. In: Proceedings of the 16th international ferro-alloys congress (INFACON XVI) 2021. Elsevier. <https://doi.org/10.2139/ssrn.3926716>
- Eidem PA, Runde M, Tangstad M, Bakken JA, Zhou Z, Yu A (2009) Effect of contact resistance on bulk resistivity of dry coke beds. *Metall Mater Trans B* 40(3):388–396
- Rooney C (2019) Homogenisation of the electrothermal behaviour of granular material. PhD thesis, University of Oxford
- Dhainaut M (2004) Proceedings of the tenth international ferroalloy congress, pp 605–613
- Eidem P (2008) Electrical resistivity of coke beds. Phd thesis, Norwegian University of Science and Technology
- “AC/DC module user’s guide,” COMSOL Multiphysics® v. 6.0, COMSOL AB, Stockholm, Sweden, 2021
- Yuferev S, Ida N (2005) Time domain surface impedance concept for low frequency electromagnetic problems-Part I: derivation of high order surface impedance boundary conditions in the time domain. *IEE Proc-Sci Meas Technol* 152(4):175–185
- Bossavit A (1999). In: Mathis W, Schindler T (eds) *Proc. ISTET’99*, vol 99, University Otto-von-Guericke, Magdeburg, Germany, 01, pp 103–107

Publisher's Note Springer Nature remains neutral with regard to jurisdictional claims in published maps and institutional affiliations.

Authors and Affiliations

Mads Fromreide^{1,2}  · Dolores Gómez^{1,3} · Sven Anton Halvorsen² · Pilar Salgado^{1,3}

✉ Mads Fromreide
mads.fromreide@rai.usc.es

¹ Department of Applied Mathematics, University of Santiago de Compostela, Campus Vida, E-15782 Santiago de Compostela, Spain

² NORCE Norwegian Research Centre AS, Universitetsveien 19, N-4630 Kristiansand, Norway

³ Galician Centre for Mathematical Research and Technology (CITMAga), Campus Vida, E-15782 Santiago de Compostela, Spain